


DHI evaluation by combining rock physics simulation and statistical techniques for fluid identification of Cambrian-to-Cretaceous clastic reservoirs in Pakistan

Nisar Ahmed¹  · Pervez Khalid¹ · Hafiz Muhammad Bilal Shafi¹ · Patrick Connolly²

Received: 26 May 2017 / Accepted: 10 August 2017 / Published online: 20 August 2017
© Institute of Geophysics, Polish Academy of Sciences & Polish Academy of Sciences 2017

Abstract The use of seismic direct hydrocarbon indicators is very common in exploration and reservoir development to minimise exploration risk and to optimise the location of production wells. DHIs can be enhanced using AVO methods to calculate seismic attributes that approximate relative elastic properties. In this study, we analyse the sensitivity to pore fluid changes of a range of elastic properties by combining rock physics studies and statistical techniques and determine which provide the best basis for DHIs. Gassmann fluid substitution is applied to the well log data and various elastic properties are evaluated by measuring the degree of separation that they achieve between gas sands and wet sands. The method has been applied successfully to well log data from proven reservoirs in three different siliciclastic environments of Cambrian, Jurassic, and Cretaceous ages. We have quantified the sensitivity of various elastic properties such as acoustic and extended elastic (EEI) impedances, elastic moduli (K_{sat} and $K_{\text{sat}}-\mu$), lambda-mu-rho method

($\lambda\rho$ and $\mu\rho$), P-to-S-wave velocity ratio (V_p/V_s), and Poisson's ratio (σ) at fully gas/water saturation scenarios. The results are strongly dependent on the local geological settings and our modeling demonstrates that for Cambrian and Cretaceous reservoirs, $K_{\text{sat}}-\mu$, EEI, V_p/V_s , and σ are more sensitive to pore fluids (gas/water). For the Jurassic reservoir, the sensitivity of all elastic and seismic properties to pore fluid reduces due to high overburden pressure and the resultant low porosity. Fluid indicators are evaluated using two metrics: a fluid indicator coefficient based on a Gaussian model and an overlap coefficient which makes no assumptions about a distribution model. This study will provide a potential way to identify gas sand zones in future exploration.

Keywords Statistical rock physics · Extended elastic impedance · Probability density function · 1D marginal distribution · Histogram · Chi angle

Introduction

Statistical rock physics analysis is normally employed to combine physical equations and statistical methods in reservoir characterization studies constrained by seismic data. One of the aims of statistics combined with rock physics is to map and predict the heterogeneities and complexities in petrophysical measurements and seismic attributes due to reservoir fluids. Therefore, the utilization of statistics in rock physics is getting to be more and more recurrent (Avseth et al. 2005; Tarantola 2005; Doyen 2007; Grana and Rossa 2010; Connolly and Hughes 2014; Grana 2014; Baddari et al. 2016). The uncertainties caused by the natural heterogeneities arising in real data can be estimating by building

✉ Nisar Ahmed
ahmedseis23@gmail.com

Pervez Khalid
pervez.geo@pu.edu.pk

Hafiz Muhammad Bilal Shafi
bilal907ahmed@yahoo.com

Patrick Connolly
patrick.connolly.451@gmail.com

¹ Institute of Geology, University of the Punjab, Lahore 54590, Pakistan

² Patrick Connolly Associates Ltd., 9 Pump Lane, Ascot, Berkshire SL5 7RW, UK

probabilistic frameworks around the theoretical or empirical relationships between reservoir and elastic properties. Grana et al. (2015) used statistical methods for facies classification by plotting Gaussian likelihoods (1D marginal distribution) and 2D confidence intervals (2D joint distributions) for various lithologies such as shale, limestone, and sandstone. Connolly (1999) exhibits the litho-fluid discrimination at shale/brine sand and shale/oil sand interfaces by portraying Gaussian probability function for acoustic (AI) and elastic (EI) impedances for shale, brine, and oil sands. These methods show that probability density functions of hydrocarbon and brine sand facies can help to define the direct hydrocarbon indicators sensitivity to pore fluids.

The use of direct hydrocarbon indicators (DHIs) from seismic data is very common in hydrocarbon prospecting and exploration strategies. Many seismic attributes have been proposed to enhance DHIs, most based on AVO behaviour (Aki and Richards 1980). These includes lambda–mu–rho (LMR) method (Goodway et al. 1997), pore space modulus (Hedlin 2000), difference in bulk (K_{sat}) and shear (μ) modulus (Batzie et al. 2001), elastic impedance (Connolly 1999) later modified as extended elastic impedance (Whitcombe et al. 2002), generalized fluid term (Russell et al. 2003), Poisson impedance (Quakenbush et al. 2006), and P-wave attenuation and dispersion (Khalid and Ahmed 2016). However, their discrimination strength varies reservoir to reservoir depending on local geological settings and control to the field data (Castagna and Smith 1994; Ahmed et al. 2015). Dillon et al. (2003) defined the fluid indicator coefficient (FIC) as the difference in mean values of attributes related to each pore fluid divided by the standard deviation of hydrocarbons saturated attribute. Higher FIC value is representative of better litho-fluid discrimination and has edge of taking into consideration as universally (best indicator) for all fluid-saturated rocks (Ahmed et al. 2016).

The objective of this work is to find the best direct hydrocarbon indicators (DHIs) for three siliciclastic reservoirs: the Khewra sandstone (Cambrian), the Datta Formation (Jurassic), and the Lower Goru Formation (Cretaceous), all onshore Pakistan. The fluid substitution analysis is performed using the well data and considers two different pore fluids, gas, and brine. In the current study, we first have applied Gassmann fluid substitution (1951) and then compute probability density functions (pdfs) of the different rock physics properties to determine the optimum fluid indicators. Histograms of data sets superimposed by probability density functions are also displayed to verify the effectiveness of Gaussians models. We calculate the fluid indicator coefficients (FICs) to quantify the

results. FICs and overlap coefficients are used also to find the best chi angles for extended elastic impedance for each reservoir.

Geological descriptions of reservoir rocks

The total sedimentary basinal area of Pakistan is about 827,000 km² and of which 10–20% has been explored. Up to June 2009, 221 out of 742 drilled exploration wells were hydrocarbon discoveries and 934 million barrels oil and 54 trillion cubic feet of gas have been exploited so far (Hydrocarbon Development Institute of Pakistan 2008; Pakistan Petroleum Information Service 2009).

Tectonically Pakistan is divided into three main basins: Baluchistan, Pishin, and Indus Basins, of which the Indus Basin is the largest and the only hydrocarbon producing basin in Pakistan. The Indus basin is subdivided into Upper (Kohat and Potwar sub Basins) and Lower (Central and Southern) Indus Basins (Kadri 1995). The Lower Indus Basin has the highest rate of discoveries in a succession of reservoir rock in small tilted fault blocks (Jamil et al. 2012).

For our current study, the Cambrian Khewra sandstone and the Jurassic Datta Formation are located in the Upper Indus Basin, while the Cretaceous Lower Goru Formation is from the Lower Indus Basin Pakistan (Fig. 1).

The Cambrian Khewra sandstone is an assemblage of thick clastic sediments well exposed in the Salt Range, Potwar area (sub-Basin in Upper Indus Basin). The Salt Range and its adjacent areas show the continental system tract and Baqri and Baloch (1991) has inferred deltaic environment of deposition for the Khewra sandstone. The Khewra Sandstone is proven reservoir in the Upper Indus Basin and has produced hydrocarbons at different fields as Rajian, Chak Naurang, and Adhi fields. The Khewra sandstone is also well developed in Punjab Platform (PPF) and encountered in different wells such as Bijnot-1 with average porosity 15%, Fort Abbas-1 (porosity about 14%), Suji-1 (porosity is about 10%), and with 6% porosity in Bahawalpur East 1 (Raza et al. 2008). However, no hydrocarbon discovery has been made in the southeastern part of PPF, and therefore, the reservoir characteristics have not been studied in detail.

The Lower Jurassic Datta Formation constitutes a significant reservoir horizon in the western Potwar and Kohat sub-Basin, where it is encountered in several oil–gas wells at the depth of more than 4 km (Kadri 1995; Shams et al. 2005). It shows a prograding deltaic facies sequence, and on the basis of proportion of sandstone detrital minerals, Datta Formation has been classified as quartzarenites. The

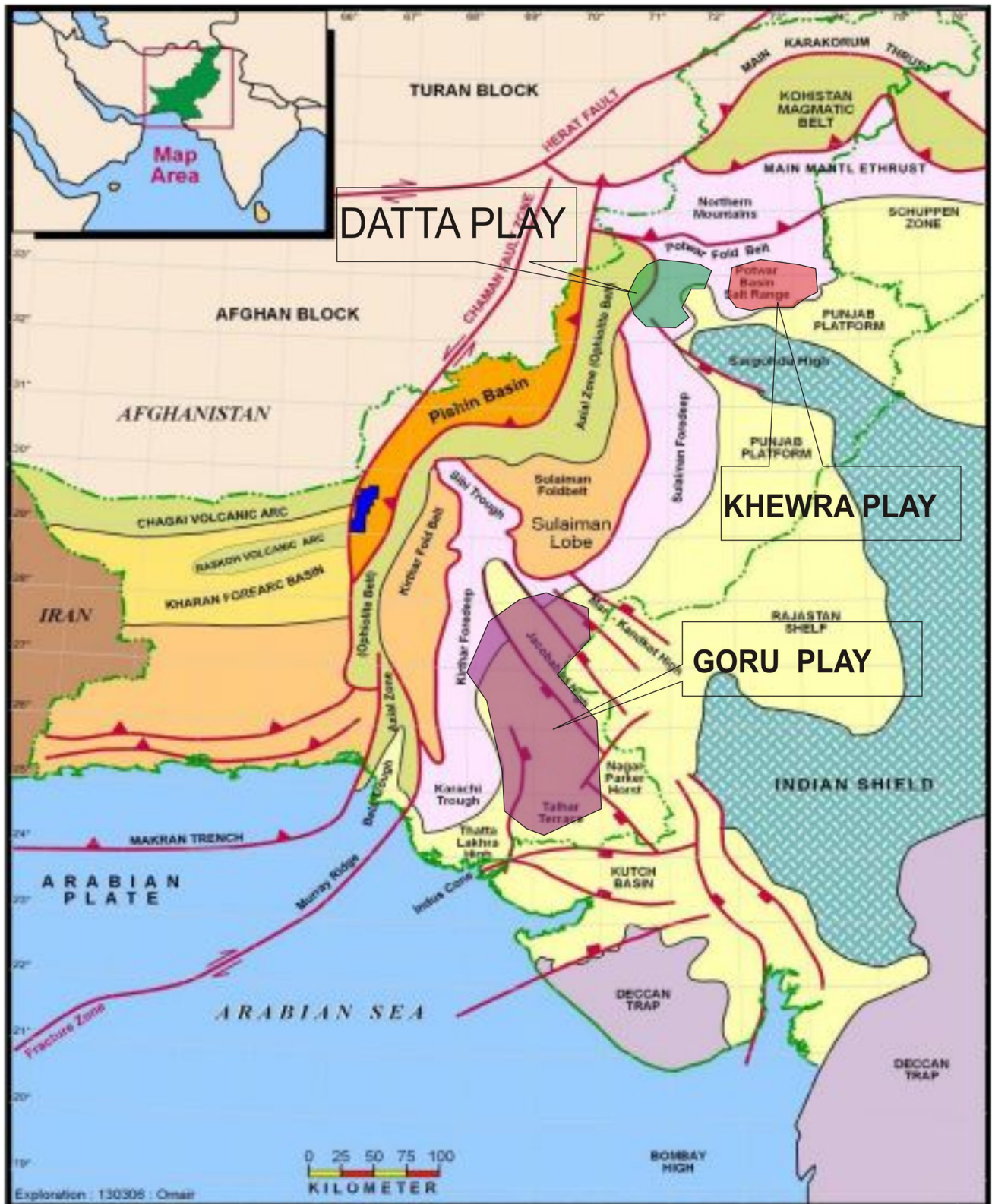


Fig. 1 Tectonic map of Pakistan. The distribution of reservoir rock in the Upper and Lower Indus Basin is also highlighted

Datta Formation is principally comprised of fine-to-coarse-grained sand particles interstratified with shales. Therefore, it has both source and reservoir rock potential. In Dhulian, the Meyal, and Toot fields located in the Potwar Plateau, Datta Formation has produced more than 15 hundred million barrels of oil, while the successful exploratory wells of Chanda and Mela fields in Datta sands in Kohat sub-Basin have made it more significant (Zaidi et al. 2013).

Clastic sediments of the Lower Goru Formation of Early Cretaceous are high-volume producers of oil, gas, and condensate in different parts of the Lower Indus Basin (Fig. 1). The Lower Goru Formation is a major plays that has contributed almost 14% of total oil and gas discoveries (Hussain et al. 2017). The Lower Indus Basin has a high success rates from a series of discoveries in comparatively small faulted blocks in the Lower Goru Formation. Recently, efforts are being made to target the stratigraphic traps in the Lower Goru Formation with some marginal success in the Lower Indus Basin. The sands of Lower Goru are primarily deposited in (lower shoreface to inner shelf settings) shallow marine environment and, therefore, have excellent reservoir characteristics (Baig et al. 2016).

Methods and theory

In this section, the mathematical theory of rock physics model and statistical algorithm to compute probability density function is described. The rock physics model permits us to calculate the elastic properties and seismic velocities from material properties such as mineralogical composition, porosity, fluid saturations and types, etc. derived from well logs by petrophysical evaluation. The effect of reservoir fluids on elastic parameters (elastic moduli) is determined by applying fluid substitution. Once we have calculated the elastic properties, seismic velocities, and density as a function of pore fluid types using fluid substitution modeling, the probability density function of the fluid indicators is estimated. The quantitative methodological framework consists of three parts: (1) petrophysical evaluation of reservoir zones; (2) fluid substitution workflow and numerical formulation of computed fluid indicators; and (3) probability density function (pdf) and calculation of fluid indicator coefficients.

Petrophysical characterization of reservoir rocks at Cambrian, Jurassic, and Cretaceous stages has been performed using available wireline log measurements of three different wells drilled in these three successions. The input wireline logs data used for present work consist of caliper, natural gamma ray (GR), density (RHOB), sonic transit

time (DT), latero log shallow (LLS) and deep (LLD), spontaneous potential (SP), neutron porosity (NPHI), etc. along with temperature data, geological formation tops, and mud filtrate resistivities. Using numerical formulas described below, the derived logs of shale volume (V_{sh}) P-wave velocity (V_p), S-wave velocity (V_s), porosity (ϕ), and water saturation (S_w) are computed. These input log measurements and derived logs are presented in results (Fig. 3).

Natural gamma ray measurements are used to identify and quantify shale volume. First, using GR measurements, linear gamma ray index (I_{GR}) is estimated, and then, substituting linear gamma ray index further into non-linear shale volume presented by Clavier et al. (1984), shale volume is estimated. These formulas are given below:

$$I_{GR} = \frac{GR_{log} - GR_{min}}{GR_{max} - GR_{min}} \quad (1)$$

$$V_{sh} = 1.7 - (3.38 - (I_{GR} + 0.7)^2)^{0.5}, \quad (2)$$

where GR_{log} , GR_{min} , and GR_{max} are gamma ray log, gamma ray minimum, and maximum values in the zone of interest, respectively.

P-wave velocity log (V_p) is derived using sonic transit time (Δt) into the relation specified below:

$$V_p \text{ (ft/s)} = \frac{1}{\Delta t \times 10^{-6}}. \quad (3)$$

The shear wave logs are not available for these wells, and therefore, various researchers (Krief et al. 1990; Gholami et al. 2014) defined algorithm to predict V_s . S-wave velocity is measured from P-wave velocity using Castagna's equation (Castagna et al. 1985):

$$V_p = 1.16V_s + 1.36. \quad (4)$$

Porosity (ϕ) log is computed by averaging density and neutron log derived porosities (Schlumberger 1997) and water saturation is estimated using the formulas given by Archie's approach (Archie 1942) and Indonesian equation (Poupon and Levieux 1971) used for clean (Eq. 5) and shaly sands (Eq. 6), respectively:

$$S_w = \sqrt{\frac{0.62}{\phi^{2.15}} \times \frac{R_w}{R_t}}, \quad (5)$$

and

$$\frac{1}{R_t} = \frac{S_w^2}{F \cdot R_w} + 2\sqrt{\frac{V_{sh}^2 - V_{sh}}{FR_w R_{sh}}} S_w^2 \frac{V_{sh}^{2-V_{cl}} S_w^2}{R_{sh}}, \quad (6)$$

where S_w , R_t , R_{sh} , and R_w are water saturation, observed total resistivity, shale resistivity, and formation water resistivity, respectively. Archie unites formation resistivity

factor (F) with the resistivity index ($R_i = R_w/R_t$). The formation resistivity factor given by Humble’s formula ($F = 0.62/\phi^{2.15}$) is the best average for sandstone reservoirs (Rider 2002).

Fluid substitution is an essential step in seismic attributes analysis and it allows us to understand how porous rock behaves seismically when its pore fluid changes. Gassmann’s equation (1951) gives a very simple relation to model pore fluid type and saturation effect on saturated bulk modulus (K_{sat}). Equations (7a) and (8) present the convenient form of Gassmann’s relations:

$$K_{sat} = K_d - \Delta K_d \tag{7a}$$

$$\Delta K_d = \frac{K_o \left(1 - \frac{K_d}{K_o}\right)^2}{1 - \phi - \frac{K_d}{K_o} + \phi \frac{K_o}{K_f}}, \tag{7b}$$

and

$$\mu_{sat} = \mu_d = \mu, \tag{8}$$

where K_d , K_o , and K_f are bulk moduli of dry rock, matrix, and fluids, respectively, and ϕ is the effective porosity of reservoir rock. μ_d and μ_{sat} are the dry and saturated rock shear moduli, respectively, and are not affected by pore fluid. ΔK_d represents the increment of bulk modulus due to fluid saturation. The bulk moduli of dry rock, matrix, and fluids are computed using the set of equations discussed by Batzle and Wang (1992) and Kumar (2006), while the effective porosity is estimated from well logs such as density and neutron. By performing the fluid substitution modeling at reservoir zones defined by well logs, two sets of saturated bulk modulus and effective density (ρ) at two different scenarios (when fully saturated either with water or gas) are calculated. This may further be used to calculate the seismic velocities of P (V_P)- and S (V_S)-wave velocities which are directly linked with bulk and shear modulus, respectively, and given by the following relations as

$$V_P = \left(\frac{K_{sat} + 4/3\mu}{\rho}\right)^{\frac{1}{2}} \tag{9}$$

and

$$V_S = \left(\frac{\mu}{\rho}\right)^{\frac{1}{2}}, \tag{10}$$

where the effective density (ρ) is the function of porosity (ϕ), matrix density (ρ_o), and fluid density (ρ_f) and is $\rho = \phi \rho_f + (1 - \phi) \rho_o$.

Using the seismic velocities and saturated bulk modulus, other rock physics properties such as acoustic impedance

($V_P \times \rho$), Poisson’s ratio ($(V_P^2 - 2V_S^2)/2(V_P^2 - V_S^2)$), and lambda ($K_{sat} - 2\mu/3$) are estimated.

Elastic impedance (EI), introduced by Connolly (1999), is the generalization of AI for non-zero incident angle and is given by the equation below:

$$EI = \left(V_P(V_P^{\tan^2 \theta} V_S^{-8K \sin^2 \theta}) \rho^{(1-4K \sin^2 \theta)}\right), \tag{11}$$

where K is a constant equal to the average value of V_S^2/V_P^2 . The original EI formula (Eq. 11) had dimensions, and hence average values, that changed with angle (theta). This problem was subsequently fixed by Whitcombe (2002) in his short note ‘Elastic Impedance Normalization’. He introduced normalisation constants, so average EI values remained the same as AI. The extended elastic impedance (EEI) equation published by Whitcombe et al. (2002) also includes normalisation constants and is given as

$$EEI(\chi) = V_{Po} \rho_o \times \left[\left(\frac{V_P}{V_{Po}}\right)^{(\cos \chi + \sin \chi)} \left(\frac{V_S}{V_{So}}\right)^{(-8K \sin \chi)} \left(\frac{\rho}{\rho_o}\right)^{(\cos \chi - 4K \sin \chi)} \right], \tag{12}$$

where V_{Po} , V_{So} , and ρ_o are the constants introduced to keep the dimensionality the same as AI and are set as the average values of P-wave velocity, S-wave velocity, and effective density of reservoir zone, respectively. We have calculated an average value of K from the normalisation constants and used single value instead of the variable K . The variable angle is now replaced with chi angle (χ) which varies between -90° and $+90^\circ$ and defined as the rotation angle in intercept–gradient space.

The normal distribution also called Gaussian distribution is an extremely important continuous probability distribution very frequently used in theory and practice. If x is the random variable, the equation of the probability density function (pdf) of Gaussian distribution is given as

$$f(x) = \frac{1}{s\sqrt{2\pi}} e^{-\frac{1}{2s^2}(x-a)^2}. \tag{13a}$$

Here, $f(x)$ is the probability density function, which gives the height of the curve at point ‘ x ’ (random variable) and a is the mean of distribution and both can take on any finite value such as $-\infty < x < \infty$. Whereas s and s^2 are the standard deviation and variance, respectively, and both must have some positive values.

To get the easier form of Gaussian distribution equation, it can be first rearranged as

$$f(x) = \frac{1}{\sqrt{2\pi}s^2} e^{-\frac{1}{2}\left(\frac{x-a}{s}\right)^2}. \tag{13b}$$

Table 1 Average of numerical values of several petrophysical properties at gross thickness levels for three sandstone reservoirs

	Khewra sandstone (Cambrian)	Datta formation (Jurassic)	Lower Goru formation (Cretaceous)
Depth (m)	2650	4735	2924.5
Reservoir thickness (m)	30	25	12
Effective porosity	0.16	0.12	0.10
Archie S_w (%)	25.09	34.73	58.09
Indonesian S_w (%)	22.09	19.99	45.89
Shale volume (%)	29	21	23

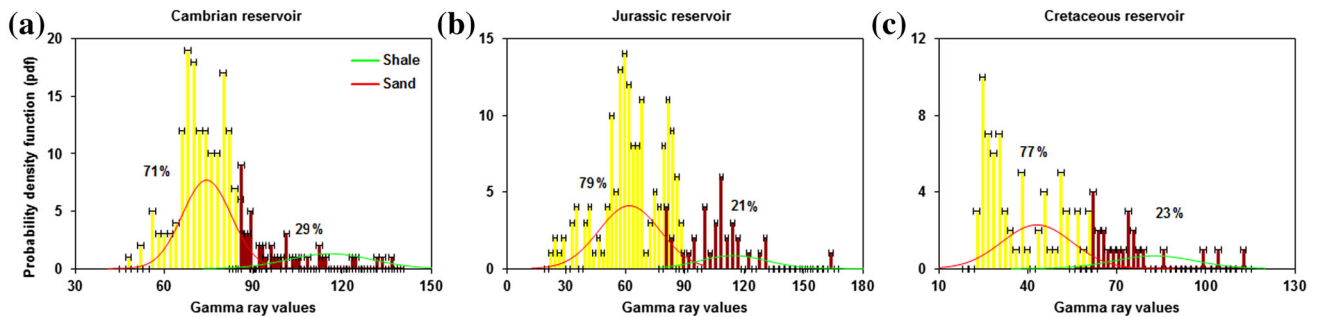


Fig. 2 Histograms with Gaussian distribution curves of gamma ray values overlaid for **a** Cambrian succession, **b** Jurassic sand, and **c** Cretaceous sandstone. The shale cut-off line for each reservoir is different and the value of shale volume varies from 21 to 29%. Shale

has higher values on gamma ray logs and lies within 70–170 API. Gaussian likelihoods functions for each facies (sand/shale) have been computed separately

This can be rearranged as

$$f(x) = \frac{1}{\sqrt{2\pi s^2}} \left(e^{\left(\frac{x-a}{s}\right)^2} \right)^{-\frac{1}{2}} \tag{13c}$$

If we consider z equal to how many standard deviations away from mean $(x - a)/s$, then the equation of the probability density function (pdf) of Gaussian distribution can be written in simplified form as

$$f(x) = \frac{1}{\sqrt{2\pi s^2 e^{-z^2}}} \tag{13d}$$

The variance (s^2) is the average of the squared deviation from mean and is calculated using following relation:

$$s^2 = \frac{\sum (x_i - a)^2}{n - 1} \tag{13e}$$

Here, x is random variable with subscript i (may be 1, 2, 3, and so on), a is the mean of all available data points (random variables), and $n - 1$ is sample size (n is total number random variables).

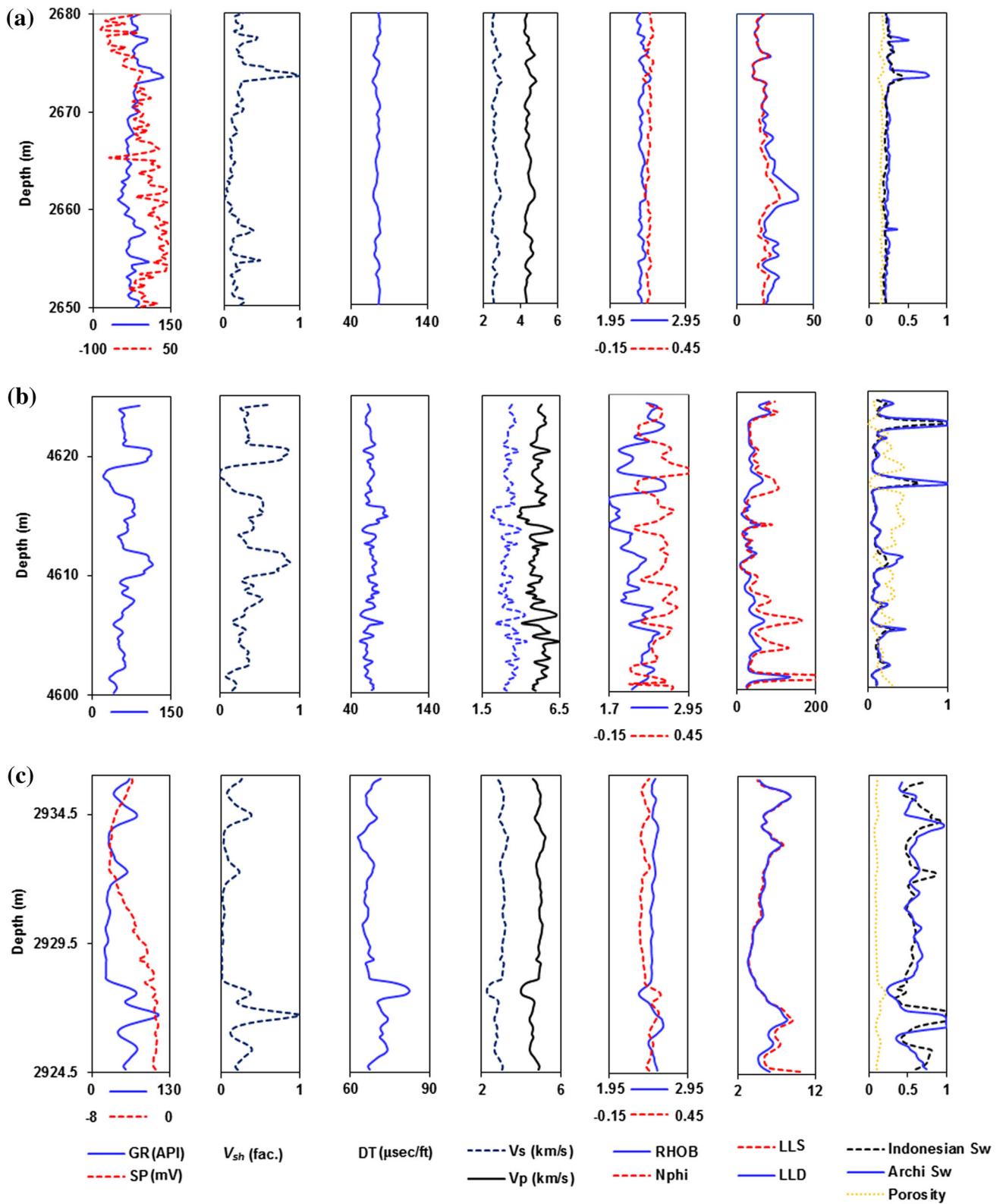
To quantify the sensitivity of each property to pore fluids, we have calculated fluid indicator coefficients (FICs). FIC is the difference between the average of the elastic property of the fully brine-saturated zone (M_{brine}) and of the fully gas-saturated zone (M_{gas}) divided by the

Fig. 3 Basic log measurements including gamma ray (GR), spontaneous potential (SP), sonic transit time (DT), density (RHOB), neutron (NPHI), latero log shallow (LLS), and petrophysically derived logs such as shale volume (V_{sh}), P- and S-wave velocities, effective porosity, and water saturation (S_w) curves are shown. These curves are computed in the reservoir zone of the entire three cases under study **a** Cambrian succession, **b** Jurassic sand, and **c** Cretaceous sandstone. All the three reservoirs mainly composed of sandstones (shale volume varies between 21 and 29%), reasonably good effective porosity (about 10–16%) and high hydrocarbon saturation (55–78%). The water saturation is computed by both Archie and Indonesian equations

standard deviation (s) of the gas-saturated zone (Dillon et al. 2003):

$$FIC = \frac{Mean_{brine} - Mean_{gas}}{s_{gas}} \tag{14}$$

The fluid indicator coefficient assumes that elastic properties for the two pore fluids are normally distributed. To test this assumption, we also measure the overlap coefficients (or Szymkiewicz–Simpson coefficient) which describes the overlap between two probability distributions without requirement of a normal distribution. Suppose X and Y are two data sets (brine sand facies and gas sand facies), then overlap coefficient is defined by dividing the



size of intersection to the smaller of the size of two data sets as

$$\text{Overlap}(X, Y) = \frac{|X \cap Y|}{\min(|X|, |Y|)}. \quad (15)$$

The intersection can be found by taking the minimum of the two sets for each histogram bin then summing that over all bins and then dividing that by the total number of samples for one of the sets (sets are both the same size in this case). The Szymkiewicz–Simpson coefficient will equal to one if X is a subset of Y .

Statistical classification of facies and reservoir fluids (gas/water)

The above-described methodology is applied to the input well log data and the results are discussed under different sections.

Facies classification and petrophysical evaluation

One of the essential steps in reservoir characterization is lithologically based facies classification to recognize the principal rock types at well locations. In the absence of depositional and sedimentological models, core analysis, and outcrop studies, the well log curves (gamma ray and spontaneous potential) are generally used to define lithologic facies (Grana et al. 2015). Rocks with clayey minerals have high values of gamma ray log as compared to clastic and carbonate rocks. The reservoir units comprise of shale and sandstone (intercalation), and therefore, gamma ray logs for each reservoir can be used to quantify the shale, as described in Table 1 and Fig. 2. All three reservoir rocks are mainly composed of sandstone with small amount of clays. Histograms and the overlying frequency (Gaussian) distribution curves for shale and sand (yellow) zones are plotted in Fig. 2.

Qualitative and quantitative evaluation of the well logs is performed and presented in Fig. 3 and Table 1. Figure 3a–c describes the input log measurements including gamma ray, sonic, density, spontaneous potential, laterolog shallow and deep, neutron porosity and derived curves of shale volume, effective porosity, and water/hydrocarbons saturation curves Cambrian, Jurassic, and Cretaceous reservoirs, respectively. The saturation of water in reservoir rock is an important parameter that is used for the evaluation of oil and gas reservoirs and many relations are available to compute it from well logs (Malureanu et al. 2016). Both the Archie (Archie 1942) and Indonesian

(Poupon and Levaux 1971) equations are used to estimate the water saturation for the Cambrian succession (Fig. 3a), Jurassic sandstone (Fig. 3b), and the Cretaceous reservoir (Fig. 3c). From Fig. 3 and Table 1, it is clear that the Archie equation overestimates the water saturation in shaley sandstones. The amount of water saturation (S_w) rises, where the shale proportion increases, because as shale volume increases, the true formation resistivity drops and S_w gets larger. Numerical values of petrophysical parameters such as effective porosity, permeability, shale volume, and water saturations for Cambrian-to-Cretaceous reservoir are given in Table 1.

Direct hydrocarbon indicators

In this section, the performance of various elastic properties that may be used as the basis for direct hydrocarbon indicators involved in exploration geophysics is examined. Using Gassmann's equation and fluid substitution algorithm described above, the behaviours log curves of different fluid indicators are calculated at two scenarios: 100% brine and 100% gas saturations are shown in Fig. 4a–c. We analyse the effectiveness of the following DHIs: EEI, AI, K_{sat} , $K_{sat}-\mu$, $\lambda\rho$, $\mu\rho$, V_p/V_s , and σ for Cambrian (Fig. 4a), Jurassic (Fig. 4b), and Cretaceous (Fig. 4c) reservoirs. Seismic AVO methods can be used to estimate relative attributes proportional to each of these with the exception of $K_{sat}-\mu$ which would require a full inversion method to estimate absolute values of K_{sat} and μ . Most of these elastic property curves show good separation for Cambrian and Cretaceous sandstones. The probability density functions derived from these are generated and discussed next.

Extended elastic and acoustic impedances

We first compare the effect of fluid substitution on acoustic and extended elastic impedances. When using EEI for fluid identification, it important to select the best chi angle. Earlier publications have used correlation coefficient to optimise chi angle (χ); however, in the current work, we have selected the best EEI angles using the fluid indicator coefficient and the overlap coefficient as described above. The results of this analysis, which are discussed in more detail below, show that a chi angle of 26° is optimal for the Cambrian reservoirs and 25° for the Jurassic and Cretaceous reservoirs. The histograms of data points overlying with Gaussian frequency curves for all three reservoir sands for gas- and brine-saturated facies are plotted in

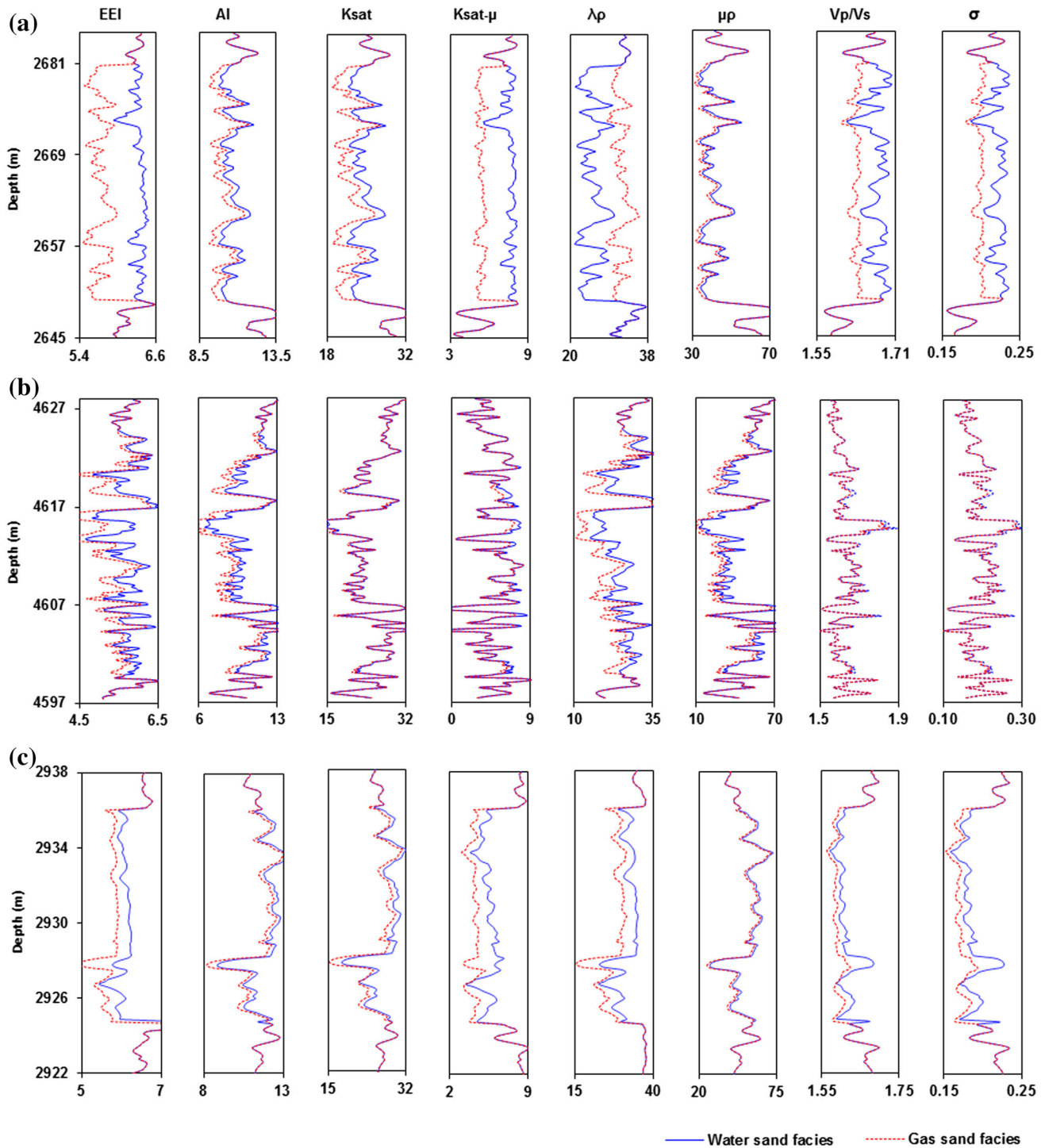


Fig. 4 Derived direct hydrocarbon indicator curves of extended elastic (EEI) and acoustic (AI) impedances, elastic moduli (K_{sat} , $K_{sat}-\mu$, $\lambda\rho$, and $\mu\rho$), and P-to-S-wave velocity ratio (V_P/V_S) and Poisson's ratio (σ) computed after performing fluid replacement modeling at

reservoir zone of Cambrian (a), Jurassic (b), and Cretaceous (c). These DHIs are computed at two different saturation levels of 100% gas and 100% brine

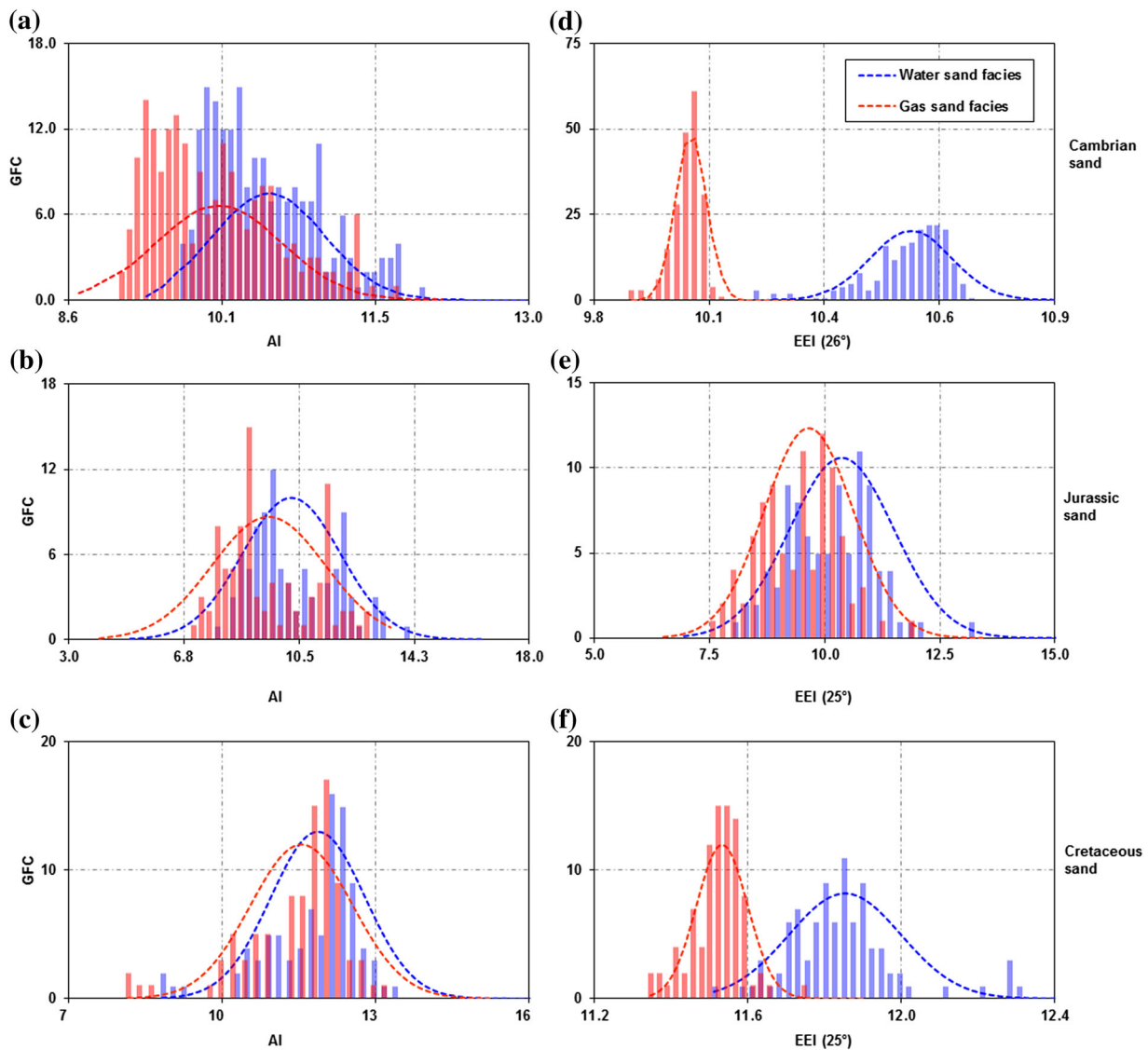


Fig. 5 Gaussian frequency curves (GFCs) and underlying histograms of acoustic (**a–c**) and extended elastic impedances (**d–f**) are plotted for Cambrian, Jurassic, and Cretaceous sands by assuming gas/water fluids. Strong overlapping of gas and brine sand GFCs (pdfs) indicates that is not a good discriminator. EEI provides maximum

differentiation between pore fluids as compared to acoustic impedance. Probability density functions and underlying data frequencies for EEIs are plotted at different chi angles for all cases. The best values of chi angles are selected after testing range of values

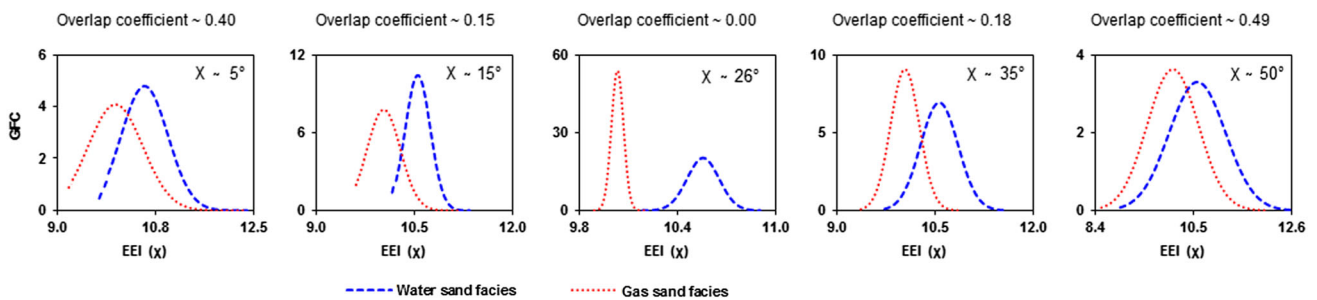


Fig. 6 Gaussian functions of extended elastic impedance for brine and gas populations at different chi angles (χ) are plotted. After testing range of values of chi angles, the best chi angle for Cambrian sand ($\chi \sim 26^\circ$) is defined, and at $\chi \sim 26^\circ$, extended elastic

impedance shows complete separation between brine and gas facies. The overlap coefficient for EEI at each chi angle is also given and has zero values at $\chi \sim 26^\circ$

Fig. 5. There is less area of overlap between gas- and water-saturated sand facies for EEI than AI. It clearly indicates that in all three cases, the extended elastic impedance is more sensitive to pore fluid types and changing saturations. However, the ability to separate the gas–water sand facies varies for each geological setting because of variations of reservoir porosity, mineralogical composition, compaction, etc. From Fig. 5a–f, it is clear that EEI is always better than AI in all three reservoirs Cambrian, Jurassic, and Cretaceous sands. The Gaussian

function and histograms for extended elastic impedance are computed and plotted at chi angle 26° (for Cambrian sand) and 25° (for Jurassic and Cretaceous sands), as shown in Fig. 5d–f.

An example of how chi angle works to describe the best option to separate fluids is shown in Fig. 6 for Cambrian case. At $\chi \sim 26^\circ$, Gaussian models have almost overlap coefficients equal to zero indicating the best option for Cambrian sand. The best options verified by plotting chi angles against fluid indicator coefficients and overlap

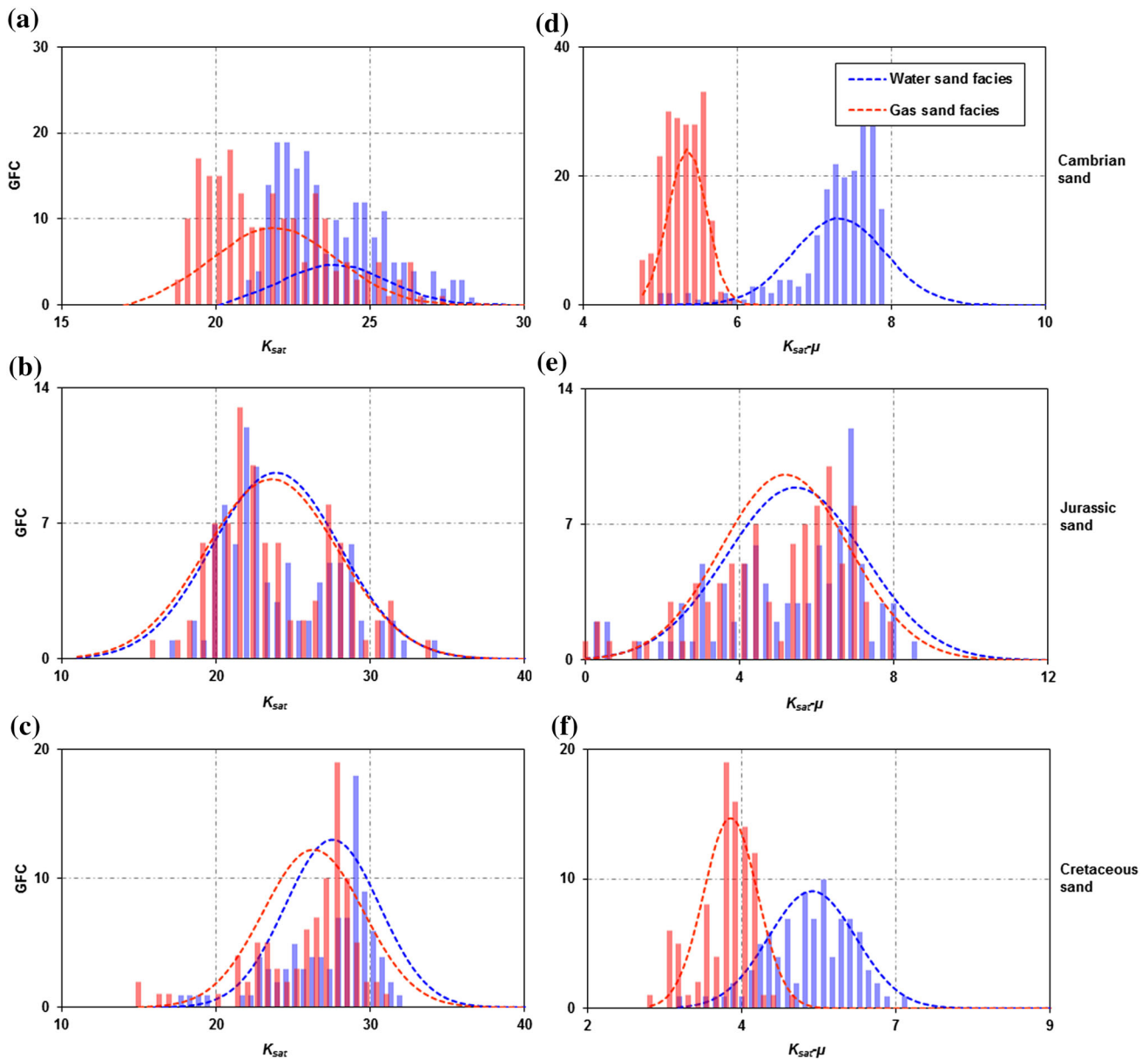


Fig. 7 1D state-conditional GFCs and underlying histograms of saturated bulk modulus (a–c) and difference in saturated bulk modulus and shear modulus (d–f) assuming that the three reservoirs are either saturated with gas (red) or water (blue). Both attributes do

not give good separation for Jurassic sandstone and show strong overlapping of GFCs. $K_{sat}\mu$ gives very good results in case of Cambrian and Cretaceous sands

coefficients (a discussion has been made in the last section of paper).

Elastic moduli

Numerous combinations of rock properties such as elastic properties and their combinations with effective density and shear modulus subtracted from saturated bulk modulus are tested. The bulk volume deformation yielded by the passage of a compressional wave causes a change in

volume of pore that results in a pressure rise of reservoir fluids (gas/water). This may stiffen the reservoir rock and cause a variation in the saturated bulk modulus. In Fig. 7, Gaussian frequency curves and histograms of data sets of saturated bulk modulus (K_{sat}) and $K_{\text{sat}}-\mu$ (also called Batzle indicator, as given by Batzle et al. 2001) for the Cambrian, Jurassic, and Cretaceous reservoirs are plotted. Sensitivity of K_{sat} to pore fluids (Fig. 7a–c) is moderate for the Cambrian sands and weak in the other two cases. Differing pore fluids has no effect on shear deformation; however,

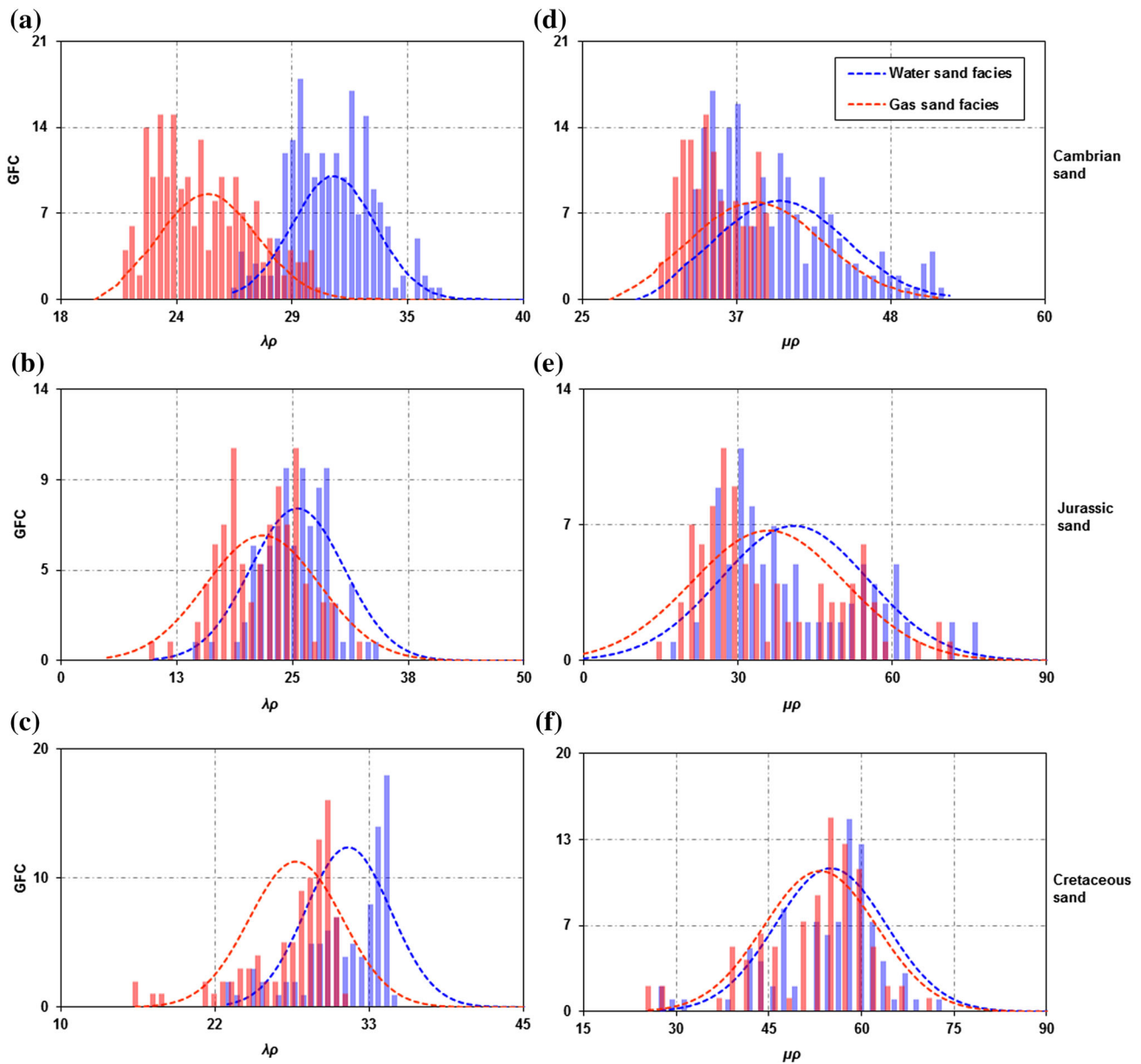


Fig. 8 Probability distribution curves and histograms of data points of $\lambda\rho$ (a–c) and $\mu\rho$ (d–f) values for wet (blue) and gas (red) sands for three different reservoirs which have geological ages from Cambrian

to Cretaceous are shown. Gaussian curves show strong overlapping for $\mu\rho$ data points, while $\lambda\rho$ is a good gas indicator which specially shows excellent discrimination in Cambrian reservoirs

when shear modulus is subtracted from saturated bulk modulus ($K_{\text{sat}}-\mu$), its pore fluid discrimination strength is increased (Fig. 7d–f). $K_{\text{sat}}-\mu$ is an excellent fluid discrimination indicator for the Cambrian sand and also works well for Cretaceous reservoirs. GFCs and histograms of both elastic properties (K_{sat} and $K_{\text{sat}}-\mu$) strongly overlap in case of Jurassic sandstone (Fig. 7b, e) and, therefore, do not work as fluid indicators. From Fig. 7, it is clearly visualized that there are some cases, where the data are a bit skewed and the Gaussian model may not be the best, but

overall data fit Gaussian model and it is a reasonable approach.

The so-called lambda–mu–rho method (Goodway et al. 1997) has been used extensively for fluid and lithology discrimination. Figure 8 shows the Gaussian frequency curves for the product of density with lambda ($\lambda\rho$) and with shear modulus ($\mu\rho$). From Fig. 8a–c, it can be inferred that $\lambda\rho$ is an excellent gas indicator for Cambrian succession and works to some extent for the Jurassic and Cretaceous sands, although there is strong overlapping of Gaussian

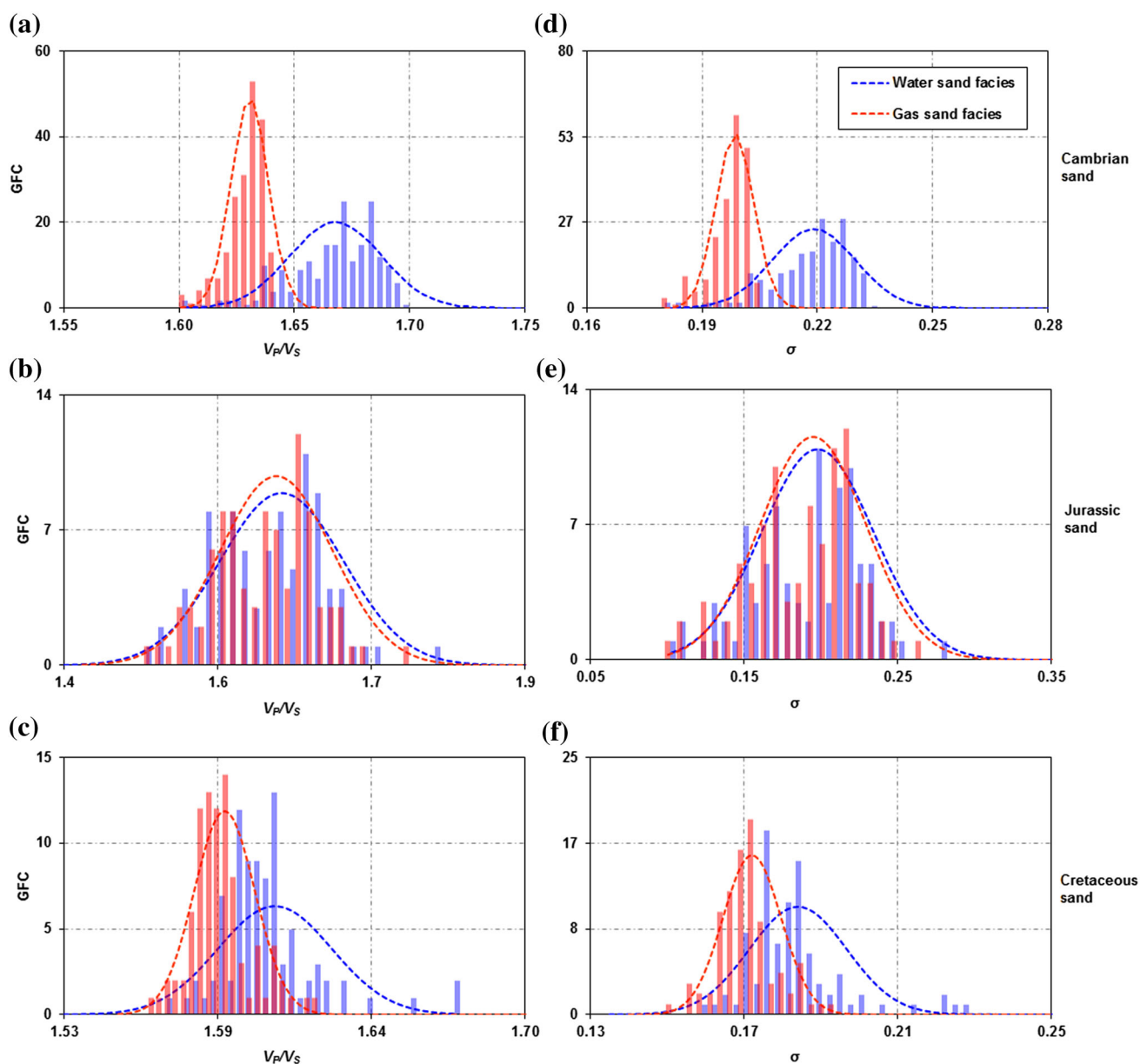


Fig. 9 Gaussian likelihoods of P-to-S-wave velocities (V_p/V_s) and Poisson's ratio (σ) for brine (blue) and gas (red) saturated and underlying histograms of data sets of Cambrian, Jurassic, and

Cretaceous sand plays are plotted. Strong overlapping clouds of 1D marginal distribution (b, e) show poor separation of gas anomalies

distributions and histograms of data points for the wet and gas sands (Fig. 8d–f). Shear modulus within the product of $\mu\rho$ does not change with fluid saturation and the GFCs only change due to the change in density.

P-to-S-wave velocities and Poisson's ratio

P-to-S-wave velocities ratio (V_P/V_S) and Poisson's ratio (σ) are often considered as helpful tools to distinguish gas-related anomalies. For an isotropic medium, σ is directly related to V_P/V_S and shows very similar trends. In Fig. 9, Gaussian frequency curves for both velocity ratio and Poisson's ratio of gas and wet zones are plotted and show very similar trend in all three reservoir plays. Both indicators also have very similar sensitivity to fluid discrimination as diagnosed graphically (Fig. 9) and numerically (Table 2). The small overlapping of Gaussian distribution curves for V_P/V_S and σ shows that they have a good chance of distinguishing wet sandstones and gas sandstones in Cambrian (Fig. 9a, d) and Cretaceous sand plays (Fig. 9c, f). However, in case of Jurassic reservoir (Fig. 9b, e), both these seismic parameters have poor chance to separate the gas sand zones as probability distribution curves strongly overlapped. However, V_P/V_S is more sensitive to fluid content than σ for all three reservoirs modeled in this study.

Fluid indicator coefficients and overlap coefficients

Fluid indicator coefficients help to analyse the sensitivity for each fluid term to discriminate reservoir fluids (gas/brine) quantitatively. These fluid indicator coefficients for Cambrian-to-Cretaceous sandstones are plotted in Fig. 10a–c and their numerical values for each property are summarized in Table 2. It can be observed that FIC values of each fluid strongly depend on local geological settings and, therefore, vary in all three reservoirs. In the case of the Cambrian sand (Fig. 10a; Table 2), $K_{\text{sat}}-\mu$, V_P/V_S , σ , and EEI (χ) have much higher FICs than all other fluid indicators which imply that these ones can easily be utilized to distinguish gas zones. Among the four seismic and elastic properties, EEI (χ) is most sensitive to pore fluid types. For Jurassic sand, except EEI (χ), all other rock physics indicators have very poor sensitivity to pore fluid content and have lower FICs values, as described in Fig. 10b and Table 2. The reason behind lower FICs may be that the Jurassic reservoir lies at the depth of 4735 m and formation pressure is 56.20 MPa. At lower pressure (higher porosity), we can have a good chance to identify and differentiate the gas-saturated sandstones. The values of FICs for Jurassic sand vary between 0.06 and 1.49 and EEI (χ) and $\lambda\rho$ have relatively higher values, as shown in Table 2. The performance of DHIs in Cretaceous sand is demonstrated in Fig. 10c and Table 2. Note that acoustic and elastic

Table 2 Numerical values of means, standard deviations, and fluid indicator coefficients (FICs) for each hydrocarbon indicator calculated at in-situ conditions are given. The fluid indicators are evaluated for three different reservoirs of Cambrian, Jurassic, and Cretaceous sandstones. Higher the values of fluid coefficients indicate better discrimination

	V_P/V_S	K_{sat}	σ	$\mu\rho$	$\lambda\rho$	$K_{\text{sat}}-\mu$	AI	EEI (χ)
Khewra sandstone (Cambrian)								
Mean water	1.66	23.86	0.21	39.93	30.96	7.32	10.51	10.55
Standard deviation water	0.02	1.70	0.01	4.96	1.98	0.59	0.53	0.098
Mean gas	1.63	21.88	0.19	38.07	24.98	5.35	10.04	10.03
Standard deviation gas	0.01	1.99	0.005	5.02	2.31	0.25	0.60	0.036
FICs	4.58	0.99	4.18	0.37	2.59	8.01	0.79	14.21
Datta sandstone (Jurassic)								
Mean water	1.63	23.87	0.19	41.13	25.37	5.34	10.25	10.27
Standard deviation water	0.07	4.13	0.04	14.83	5.03	2.02	1.59	0.45
Mean gas	1.63	23.60	0.19	36.10	21.64	5.08	9.51	9.53
Standard deviation gas	0.06	4.28	0.03	15.26	6.11	1.91	1.84	0.48
FICs	0.09	0.06	0.08	0.32	0.61	0.13	0.40	1.49
Lower Goru (Cretaceous)								
Mean water	1.60	27.53	0.18	54.94	31.68	5.39	11.86	11.55
Standard deviation water	0.02	3.06	0.01	8.96	3.20	0.66	0.92	0.146
Mean gas	1.59	26.30	0.17	53.32	27.76	4.16	11.55	11.53
Standard deviation gas	0.01	3.25	0.01	9.16	3.53	0.41	1.00	0.066
FICs	1.66	0.37	1.58	0.18	1.11	3.03	0.32	4.80

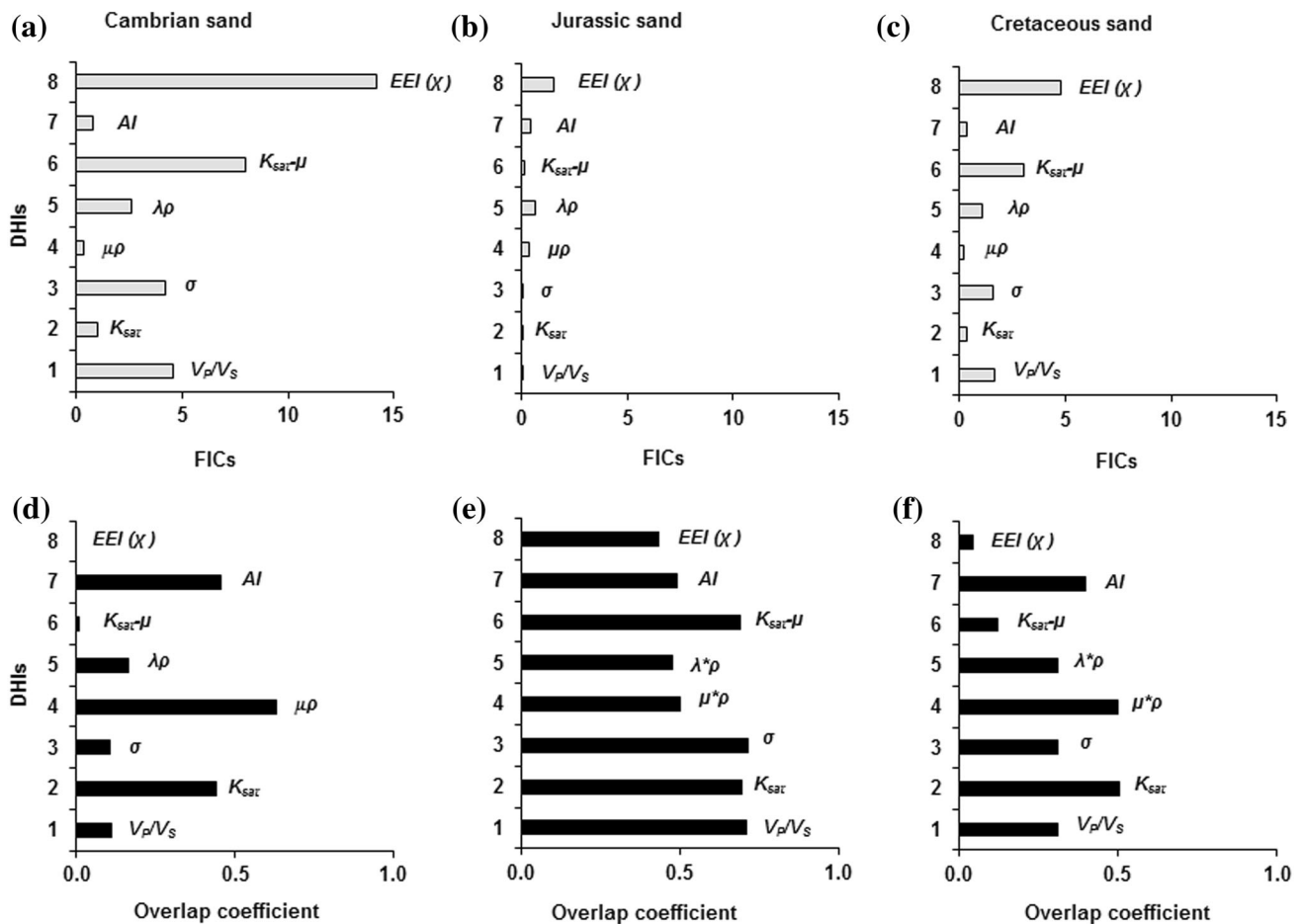


Fig. 10 FIC values of different attributes (a–c) for three reservoirs at the same scale are plotted. Most of the fluid indicators have very low values of fluid coefficients for Jurassic sands indicating that are less sensitive to pore fluids (b). Higher the values of fluid coefficients

mean excellent distinguisher of hydrocarbons facies. The overlap coefficients of brine and gas-saturated data sets for each attribute of three reservoirs are computed (d–f). The fluid indicators having higher FICs values show lower overlap coefficients

Table 3 Overlap coefficients (Szymkiewicz–Simpson coefficient) are given for each attribute of three reservoirs. Higher overlap coefficient values of fluid indicators indicate that both water and gas facies have less chance to distinguish

Overlap coefficients	V_p/V_s	K_{sat}	σ	$\mu\rho$	$\lambda\rho$	$K_{sat}-\mu$	AI	EEI (χ)
Cambrian sand	0.11	0.44	0.10	0.63	0.16	0.02	0.45	0.00
Jurassic sand	0.70	0.69	0.71	0.50	0.47	0.69	0.48	0.45
Cretaceous sand	0.31	0.51	0.31	0.50	0.31	0.12	0.40	0.05

properties EEI (χ) and $K_{sat}-\mu$ yielded excellent results to discriminate the gas sand zone from water-saturated zone. Some other properties such as V_p/V_s and σ are obviously more diagnostic than remaining.

As the name suggests, the overlap coefficients measure the degree of overlap between two populations or probability distributions. A smaller overlap coefficient for the two populations (wet sand and gas sand) indicates good separation and vice versa. The overlap coefficients for each property computed at two saturation limits for all the three clastic reservoirs are plotted in Fig. 10d (Cambrian sand),

Fig. 10e (Jurassic sand), and Fig. 10f (Cretaceous sand) and their numerical values are given in Table 3. The overlap coefficient analysis and the FIC analysis are in good agreement.

Chi angle (χ) versus fluid indicator coefficients and overlap coefficients

Extended elastic impedance is a function of chi, the rotation angle in intercept–gradient space. The value of chi must be optimised for whatever purpose EEI is being used

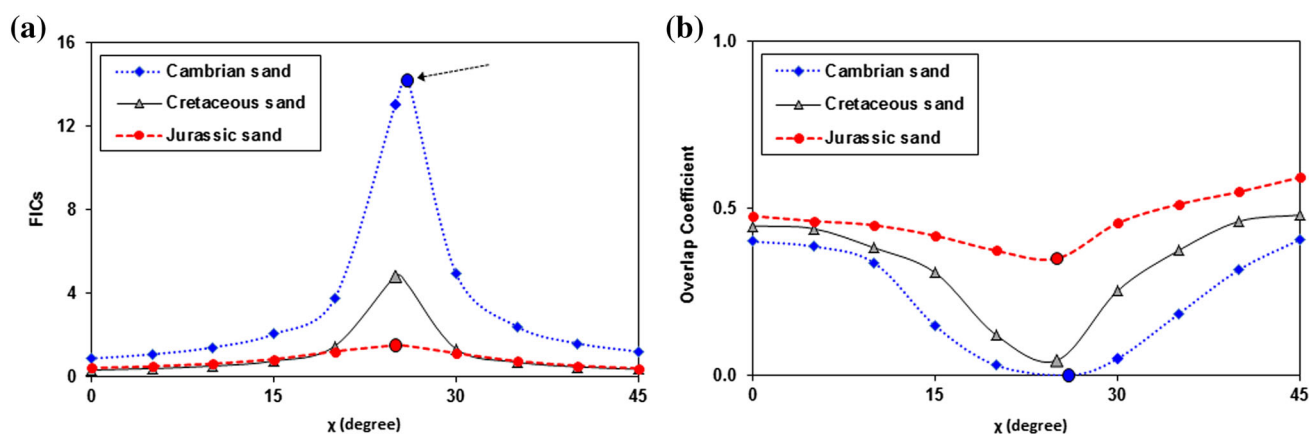


Fig. 11 **a** FICs are computed against a range of chi angles for three cases and plotted to select the best option. For Cambrian, Jurassic, and Cretaceous sands, the higher FICs are against 26°, 25°, and 25° chi

angles, respectively. **b** Best chi angle option does not change when it is plotted against overlap coefficients. At 26°, 25°, and 25° chi angles, the overlap coefficients have lower values

in the case of fluid discrimination. In this study, we optimised chi by measuring the FICs and the overlap coefficients for a range of chi values. FIC values and overlap coefficients for chi angles from 0°–45° are shown in Fig. 11a, b, respectively. The optimum angles exhibit a high FIC and a low overlap coefficient and both are in good agreement.

Conclusions

Quantitative analysis of three siliciclastic reservoirs has demonstrated that acoustic and elastic property reservoir rocks are strongly affected by pore fluid types. However, the sensitivity of the properties varies with the nature of the reservoir depending on various reservoir properties. Fluid indicator coefficients (FICs) and overlap coefficients provide an effective way of determining the degree of sensitivity for a range of elastic properties. Relative changes in elastic properties can be estimated using AVO techniques, and hence, an analysis of FICs and overlap coefficients will show which of these will be most useful as DHIs and will indicate the potential quality of the DHIs for different reservoirs. We have also demonstrated that fluid indicator and overlap coefficients can be used to optimise the extended elastic impedance chi angle for fluid discrimination.

In all cases, the optimised EEI proved to be most sensitive to changes in pore fluid, but the sensitivity varied considerably between the three reservoirs. The high porosity, shallow Khewra sandstone of Cambrian age, was most sensitive and the deeper, lower porosity Jurassic Datta sand the least sensitive. This study can suggest optimal ways to identify gas sand zones when exploration is carried in the future for the Cambrian, Jurassic, and Cretaceous reservoirs.

Acknowledgements The authors would like to acknowledge to Directorate General Petroleum Concessions (DGPC) for providing data to complete the present work. The Institute of Geology, University of the Punjab is also acknowledged for facilitating me in the compilation of this work. This research paper is from the Ph.D. work of Mr. Nisar Ahmed, Lecturer, Institute of Geology, University of the Punjab.

References

- Ahmed N, Khalid P, Ghazi S, Anwar AW (2015) AVO forward modeling and attributes analysis for fluid's identification: a case study. *Acta Geod Geophys* 50(4):377–390. doi:[10.1007/s40328-014-0097-x](https://doi.org/10.1007/s40328-014-0097-x)
- Ahmed N, Khalid P, Ali T, Ahmad SR, Akhtar S (2016) Differentiation of pore fluids using amplitude versus offset attributes in clastic reservoirs, Middle Indus Basin, Pakistan. *Arab J Sci Eng* 41(6):2315–2323. doi:[10.1007/s13369-015-1992-3](https://doi.org/10.1007/s13369-015-1992-3)
- Aki K, Richards PG (1980) *Quantitative seismology: theory and methods*. W. H. Freeman, San Francisco
- Archie GE (1942) The electrical resistivity log as an aid in determining some reservoir characteristics. *Trans Am Inst Mech Eng* 146(1):54–62
- Avseth P, Mukerji T, Mavko G (2005) *Quantitative seismic interpretation*. Cambridge University Press, Cambridge
- Baddari K, Bellalem F, Baddari I, Makdeche S (2016) Some probabilistic and statistical properties of the seismic regime of Zemmouri (Algeria) seismogenic zone. *Acta Geophys* 64(5):1275–1310. doi:[10.1515/acgeo-2016-0049](https://doi.org/10.1515/acgeo-2016-0049)
- Baig MO, Harris NB, Ahmed H, Baig MOA (2016) Controls on reservoir diagenesis in the Lower Goru Sandstone Formation, Lower Indus Basin, Pakistan. *J Petrol Geol* 39(1):29–48. doi:[10.1111/jpg.12626](https://doi.org/10.1111/jpg.12626)
- Baqri SRH, Baloch MQ (1991) Sedimentological studies and palaeo environments of Khewra Sandstone with reference to its hydrocarbon potential. *Pak J Pet Technol Altern Fuels* 1:23–38
- Batzle ML, Wang Z (1992) Seismic properties of pore fluids. *Geophysics* 57(11):1396–1408. doi:[10.1190/1.1443207](https://doi.org/10.1190/1.1443207)
- Batzle ML, Han DH, Hofmann R (2001) Optimal hydrocarbon indicators. In: 71th SEG international exposition and annual meeting 2001, September 9–14, 2001, San Antonio. doi:[10.1190/1.1816446](https://doi.org/10.1190/1.1816446)

- Castagna JP, Batzle ML, Eastwood RL (1985) Relationships between compressional and shear-wave velocities in clastic silicate rocks. *Geophysics* 50(4):551–570. doi:[10.1190/1.1441933](https://doi.org/10.1190/1.1441933)
- Castagna JP, Smith SW (1994) Comparison of AVO indicators: a modeling study. *Geophysics* 59(12):1849–1855. doi:[10.1190/1.1443572](https://doi.org/10.1190/1.1443572)
- Clavier C, Coates G, Dumanoir J (1984) The theoretical and experimental basis for the ‘dual water’ model for the interpretation of shaly sands. *Soc Pet Eng J* 24(2):153–168. doi:[10.2118/6859-PA](https://doi.org/10.2118/6859-PA)
- Connolly P (1999) Elastic impedance. *Lead Edge* 18(4):438–452. doi:[10.1190/1.1438307](https://doi.org/10.1190/1.1438307)
- Connolly P, Hughes M (2014) The application of very large numbers of pseudo-wells for reservoir characterization. Society of Petroleum Engineers 2014, SPE-171879-MS, November 10–13, 2014, Abu Dhabi. doi:[10.2118/171879-MS](https://doi.org/10.2118/171879-MS)
- Dillon L, Schwedersky G, Vasquez G, Velloso R, Nunes C (2003) A multiscale DHI elastic attributes evaluation. *Lead Edge* 22(10):1024–1029. doi:[10.1190/1.1623644](https://doi.org/10.1190/1.1623644)
- Doyen P (2007) Seismic reservoir characterization. EAGE, Netherlands
- Gassmann F (1951) Über die elastizität poröser medien. *Verteljahrsschrift der Naturforschenden Gesellschaft in Zurich* 96:1–23
- Gholami R, Moradzadeh A, Rasouli V, Hanachi J (2014) Shear wave velocity prediction using seismic attributes and well log data. *Acta Geophys* 62(4):818–848. doi:[10.2478/s11600-013-0200-7](https://doi.org/10.2478/s11600-013-0200-7)
- Goodway W, Chen T, Downton J (1997) Improved AVO fluid detection and lithology discrimination using Lamé petrophysical Parameters; “Lambda-Rho”, “Mu-Rho”, and “Lambda/Mu fluid stack”, from P and S inversions. In: 67th SEG annual international meeting 1997, November 2–7, 1997, Dallas. doi:[10.1190/1.1885795](https://doi.org/10.1190/1.1885795)
- Grana D (2014) Probabilistic approach to rock physics modeling. *Geophysics* 79(2):D123–D143. doi:[10.1190/GEO2013-0333.1](https://doi.org/10.1190/GEO2013-0333.1)
- Grana D, Rossa ED (2010) Probabilistic petrophysical-properties estimation integrating statistical rock physics with seismic inversion. *Geophysics* 75(3):O21–O37. doi:[10.1190/1.3386676](https://doi.org/10.1190/1.3386676)
- Grana D, Schlanser K, Campbell-Stone E (2015) Petroelastic and geomechanical classification of lithologic facies in the Marcellus Shale. *Interpretation* 3(1):SA51–SA63. doi:[10.1190/INT-2014-0047.1](https://doi.org/10.1190/INT-2014-0047.1)
- Hedlin K (2000) Pore space modulus and extraction using AVO. In: 70th SEG annual international meeting 2000, August 6–1, 2000, Calgary. doi:[10.1190/1.1815749](https://doi.org/10.1190/1.1815749)
- Hussain M, Ahmed N, Chun WY, Khalid P, Mahmood A, Ahmad SR, Rasool U (2017) Reservoir characterization of basal sand zone of lower Goru formation by petrophysical studies of geophysical logs. *J Geol Soc India* 89(3):331–338. doi:[10.1007/s12594-017-0614-y](https://doi.org/10.1007/s12594-017-0614-y)
- Hydrocarbon Development Institute of Pakistan (2008) Energy Year Book, 2008. Ministry of Petroleum and Natural Resources, Pakistan
- Jamil A, Waheed A, Sheikh RA (2012) Pakistan’s major petroleum plays: an overview of dwindling reserves. Search and Discovery article #10399 (2012), PAPG/SPE Annual Technical Conference 2009, December 03–05, 2012, Islamabad
- Kadri IB (1995) Petroleum geology of Pakistan. Pakistan Petroleum Ltd, Karachi
- Khalid P, Ahmed N (2016) Modulus defect, velocity dispersion and attenuation in partially-saturated reservoirs of Jurassic sandstone, Indus Basin, Pakistan. *Stud Geophys Geod* 60(1):112–129. doi:[10.1007/s11200-015-0804-2](https://doi.org/10.1007/s11200-015-0804-2)
- Krief M, Garat J, Stellingwerff J, Ventre J (1990) A petrophysical interpretation using the velocities of P and S waves (full-waveform sonic). *Log Analyst* 31(8):355–369
- Kumar D (2006) A Tutorial on Gassmann fluid substitution: formulation, algorithm and matlab code. *Geohorizons* 11(1):4–12
- Malureanu I, Boaca T, Daniela-Doina N (2016) New relations of water saturation’s Calculus from well logs. *Acta Geophys* 64(5):1542–1562. doi:[10.1515/acgeo-2016-0063](https://doi.org/10.1515/acgeo-2016-0063)
- Pakistan Petroleum Information Service (2009) Upstream Petroleum activities. Ministry of Petroleum and Natural Resources
- Poupon A, Levieux J (1971) Evaluation of water saturation in shaly formations. Society of Professional Well Log Analysts 12th annual logging symposium transactions, Paper O
- Quakenbush M, Shang B, Tuttle C (2006) Poisson impedance. *Lead Edge* 25(2):128–138. doi:[10.1190/1.2172301](https://doi.org/10.1190/1.2172301)
- Raza HA, Ahmad W, Ali SM, Mujtaba M, Alam S, Shafeeq M, Iqbal M, Noor I, Riaz N (2008) Hydrocarbon prospects of Punjab Platform Pakistan, with special reference to Bikaner-Nagaur Basin of India, Pakistan. *J Hydrocarbon Res* 18(6):1–33
- Rider MH (2002) The geological interpretation of well logs. Rider French Consulting Ltd, Sutherland
- Russell B, Hedlin K, Hilterman F, Lines L (2003) Fluid-property discrimination with AVO: a Biot–Gassmann perspective. *Geophysics* 68(1):29–39. doi:[10.1190/1.1543192](https://doi.org/10.1190/1.1543192)
- Schlumberger (1997) Log interpretation charts. Schlumberger well services, Houston
- Shams O, Qureshi AW, Abbasi IA (2005) Lithofacies, sand-bodies geometry and depositional setting of the Datta Formation in Surghar Range, North Pakistan. In: Annual technical conference 2005, November 21–23, 2005, Islamabad
- Tarantola A (2005) Inverse problem theory. SIAM, Paris, France
- Whitcombe DN (2002) Elastic impedance normalization. *Geophysics* 67(1):60–62. doi:[10.1190/1.1451331](https://doi.org/10.1190/1.1451331)
- Whitcombe DN, Connolly PA, Reagan RL, Redshaw TC (2002) Extended elastic impedance for fluid and lithology prediction. *Geophysics* 67(1):63–67. doi:[10.1190/1.1451337](https://doi.org/10.1190/1.1451337)
- Zaidi SNA, Brohi IA, Ramzan K, Ahmed N, Mehmood F, Brohi AU (2013) Distribution and hydrocarbon potential of Datta Sands in Upper Indus Basin, Pakistan. *Sindh Univ Res J* 45(2):325–332